Locking of length scales in two-band superconductors

M. Ichioka, V. G. Kogan, and J. Schmalian

Phys. Rev. B **95**, 064512 — Published 21 February 2017

DOI: 10.1103/PhysRevB.95.064512

Locking of length scales in two-band superconductors

M. Ichioka
*Department of Physics, RIIS, Okayama University, Okayama 700-8530, Japan**

V. G. Kogan
Ames Laboratory, US Department of Energy, Ames, Iowa 50011, USA

J. Schmalian
Institut für Theorie der Kondensierten Materie und Institut für Festkörperphysik, Karlsruher Institut für Technologie, D-76131 Karlsruhe, Germany

(Dated: January 30, 2017)

A model of a clean two-band s-wave superconductor with cylindrical Fermi surfaces, different Fermi velocities $v_{1,2}$, and a general 2×2 coupling matrix $V_{\alpha\beta}$ is used to study the order parameter distribution in vortex lattices. The Eilenberger weak coupling formalism is used to calculate numerically the spatial distributions of the pairing amplitudes Δ_1 and Δ_2 of the two bands for vortices parallel to the Fermi cylinders. For generic values of the interband coupling V_{12}, it is shown that, independently of the couplings $V_{\alpha\beta}$, of the ratio v_1/v_2, of the temperature, and the applied field, the length scales of spatial variation of Δ_1 and of Δ_2 are the same within the accuracy of our calculations. The only exception from this single length-scale behavior is found for $V_{12} \ll V_{11}$, i.e., for nearly decoupled bands.

PACS numbers: 74.20.-z, 74.25.Uv

I. INTRODUCTION

Just at the dawn of the theory of multiband superconductors, it was established that near the critical temperature T_c the length scales of spatial variation of the pairing amplitudes of the bands, are in fact the same, notwithstanding differences in zero-T BCS coherence lengths $\xi_{0,\alpha} \propto v_\alpha/T_c$ (α is the band index and v_α is the Fermi velocity)[1]. This result has been "rediscovered" in the recent debate on the proper form of Ginzburg-Landau (GL) theory of two-band superconductors[2,3]. The debate was triggered by extensive studies of multiband MgB_2 which prompted the formulation of two order-parameter GL energy functionals to allow for different length scales $\xi_1 \neq \xi_2$ associated with the two underlying bands, see Refs. [4,5] and references therein.

There are different definitions of the coherence length in literature. To avoid misunderstanding we note upfront that in this work we consider the spatial distributions of pair-potentials within vortex lattices, in which the natural length scales of pair potentials is the size of the vortex core, $\xi^{(c)}$. We define this size via the relation

$$\frac{|\Delta_{m,\alpha}|}{\xi_\alpha^{(c)}} = \frac{d|\Delta_\alpha|}{dr}\Big|_{r\to 0}, \quad \alpha = 1, 2 \tag{1}$$

along a radius r from a vortex center. Here α is the band index, $\Delta_{m,\alpha}$ is the maximum value of the pair potential within the vortex lattice (in hexagonal lattices of interest here it is reached at the center of the equilateral vortex triangle). In one band materials, $\xi^{(c)}$ and the coherence length ξ are of the same order, whatever definition of ξ is adopted. We also note that $\xi_\alpha^{(c)}$ differ from lengths governing asymptotic behavior of Δ_α at $r \to \infty$ studied in Ref. [5] because within vortex lattices in finite fields r is restricted by the finite unit cell size. Also, $\xi_\alpha^{(c)}$ differ from somewhat artificial "healing lengths" of Ref. [6], although these lengths and $\xi_\alpha^{(c)}$ are of the same order.

While it is established that near T_c, where the GL-expansion is justified, any superconductor with finite interband coupling is governed by a single superconducting order parameter with one coherence length, this does not have to be true away from T_c. Novel behavior is expected especially in cases with different Fermi velocities of the bands and for very weak interband coupling; this requires to turn to microscopic descriptions of superconductors applicable at all temperatures. Calculations of this kind showed[6,7] that away from T_c and for a very weak interband coupling the length scales ξ_1 and ξ_2 are indeed not equal, in particular for low temperatures and at small magnetic fields. The work on the two-band Extended GL formalism also showed different bands coherence lengths depending on material parameters; this formalism, however, cannot be extended all the way to $T = 0$[8].

However, there are several reasons why in real materials the interband coupling is not weak. First, the ever present Coulomb repulsion will inevitably give rise to off-diagonal matrix elements in band-representation, even-though the usual renormalization of the Coulomb pseudopotential tends to reduce interband interactions more strongly than intraband couplings[9]. For MgB_2 the latter effect is rather moderate[9]: the bare interband Coulomb interaction is about half of the bare intraband interaction; renormalizations only reduce this ratio by another factor of 2, yielding interband Coulomb interactions that are approximately 25% of the intraband couplings. Second, the matrix elements of the electron-lattice coupling within and between electronic bands are for the impor-

tant optical phonon branches a priori of the same order of magnitude. Even for MgB_2, where the Raman spectrum[10] suggests existence of a Leggett-mode along with comparatively weak interband coupling, a careful analysis of the inter- and intra-band interactions reveals that the former is still about 20% of the larger and similar to the smaller of the intraband interactions[9,11–14]. In other systems, such as the recently discussed iron-based superconductors, it is even argued that the interband coupling is the dominant source of pairing, see e.g. Refs.[15,16].

Further support for comparatively large interband coupling comes from an analysis of recent Scanning Tunneling Microscopy (STM) measurements of the density of states (DOS) distribution within the vortex lattice at low temperatures in several two-band compounds[17,18]. For a single-band material one can construct a phenomenological model to relate the measured zero-bias DOS distribution $N(\boldsymbol{r})$ to the pairing amplitudes $|\Delta(\boldsymbol{r})|$ in the lattice unit cell[17]. This procedure is readily extended to a two-band situation, for which $N(\boldsymbol{r})$ depends on both $\xi_1^{(c)}$ and $\xi_2^{(c)}$. The fit to the STM data for $NbSe_2$ and for $NbSe_{1.8}S_{0.2}$ showed that $\xi_1^{(c)} \approx \xi_2^{(c)}$ at $T = 0.15\,\mathrm{K} \ll T_c$. The same procedure has been applied to the novel superconductor $CaKFe_4As_4$ with $T_c \approx 35\,\mathrm{K}$ and the zero-field tunneling spectrum having clearly two-gap features, again with the result $\xi_1^{(c)} \approx \xi_2^{(c)}$ at sub-Kelvin temperatures and at all fields examined[18].

These theoretical considerations and observations motivated us to re-examine the question of the relative values of $\xi_1^{(c)}$ and $\xi_2^{(c)}$ in two-band superconductors within a microscopic approach that covers a broad temperature and magnetic field regime. In particular, the analysis of the STM-data suggests that the emergence of one common length-scale is a much more robust phenomenon than one would expect for moderately coupled multiband system. Thus, we aim at clarifying the issue of when the coupling between two superconducting bands becomes sufficiently strong to give rise to a common length scale and under what conditions two separate length scales of the band-order parameters emerge.

To this end, we use a "brute-force" numerical procedure of solving Eilenberger equations for a vortex lattice in the two-band case developed in studies of MgB_2[19], and estimate temperature and magnetic field dependences of the vortex core sizes. We consider a weak-coupling model of a two-band superconductor with two Fermi surface parts having different Fermi velocities and study the spatial variation of the pairing amplitudes $\Delta_{1,2}(\boldsymbol{r})$ of the two bands within the vortex lattice unit cell. While we analyze this model over a wide range of parameters, we do not focus on a specific application for a particular material. Rather, we intend to clarify general properties of the spatial dependence of $\Delta_{1,2}(\boldsymbol{r})$. Substantially different values of the Fermi velocities notwithstanding, the coherence lengths proportional to the vortex core sizes defined in Eq. (1) turn out nearly the same for all choices of coupling constants $V_{\alpha\beta}$ examined ($\alpha, \beta = 1, 2$) except the case of nearly decoupled condensates $V_{12}/V_{11} < 0.1$.

For $V_{12} \ll V_{11}$ our results agree with previous calculations[6–8]. However, as soon as $V_{12}/V_{11} \geq 0.1$, we obtain $\xi_1^{(c)} \approx \xi_2^{(c)}$, insensitive to details of coupling $V_{\alpha\beta}$, temperature, and field.

II. APPROACH

We consider two-band system with two cylindrical Fermi surfaces ($\alpha = 1, 2$) both oriented parallel to the same crystal axis (the c -axis) and with Fermi velocities $\boldsymbol{v}_\alpha(\boldsymbol{k}) = v_\alpha(\cos\phi, \sin\phi)$. $\boldsymbol{k}$ is the Fermi momentum and ϕ the corresponding azimuth. The magnetic field is applied along $\boldsymbol{c}$ as well, i.e. the field is parallel to the axis of the cylinder. For simplicity, the bands normal densities of states are assumed the same: $N_{0,1} = N_{0,2} = N_0$ (the total DOS per spin $N(0) = 2N_0$). This assumption will not affect any of our results qualitatively and can easily be dropped. It still allows for distinct values of the Fermi velocities of the bands. We set $v_2 = 3v_1$ to assure substantially different coherence lengths in the limit of fully decoupled bands. The 2×2 coupling matrix $V_{\alpha\beta}$ is assumed symmetric: $V_{12} = V_{21}$.

Our approach is based on the quasiclassical version of the weak-coupling BCS theory for anisotropic Fermi surfaces and order parameters[20]. This theory is formulated in terms of Eilenberger functions f, f^+ and g (Gor'kov's Green's functions averaged over the energy):

$$(2\omega + \boldsymbol{v}_\alpha \cdot \boldsymbol{\Pi}) f_\alpha = 2\Delta_\alpha g_\alpha\,, \tag{2}$$

$$g_\alpha^2 = 1 - f_\alpha f_\alpha^+\,, \qquad \alpha = 1, 2. \tag{3}$$

Here $\boldsymbol{\Pi} = \boldsymbol{\nabla} + 2\pi i \boldsymbol{A}/\phi_0$ with vector potential $\boldsymbol{A}$ and flux quantum ϕ_0. $\omega = \pi T(2n+1)$ are fermionic Matsubara frequencies with integer n; hereafter ω and T are measured in energy units, i.e. $\hbar = k_B = 1$. The equation for f^+ is obtained from Eq. (2) by taking the complex conjugate and replacing $\boldsymbol{v} \to -\boldsymbol{v}$.

The pairing amplitudes satisfy the self-consistency relations:

$$\Delta_\alpha(\boldsymbol{r}) = 4\pi T N_0 \sum_{\beta,\,\omega} V_{\alpha\beta} \langle f(\omega, \boldsymbol{k}, \boldsymbol{r}) \rangle_\beta\,, \tag{4}$$

where the sum over positive Matsubara frequencies is extended up to ω_D, the analog of Debye frequency for electron-phonon mechanism; $\langle f(\omega, \boldsymbol{k}, \boldsymbol{r}) \rangle_\beta$ stands for the average over the Fermi cylinder of the band β. The contribution of the α-band to the current density is

$$\boldsymbol{J}_\alpha(\boldsymbol{r}) = -4\pi|e|N_0 T\,\mathrm{Im} \sum_{\omega>0} \langle \boldsymbol{v} g(\omega, \boldsymbol{k}, \boldsymbol{r}) \rangle_\alpha\,, \tag{5}$$

and the total current density is

$$\boldsymbol{J} = \boldsymbol{J}_1 + \boldsymbol{J}_2 = \boldsymbol{\nabla} \times (\boldsymbol{\nabla} \times \boldsymbol{A})\, c/4\pi\,. \tag{6}$$

The vector potential is taken in the form $\boldsymbol{A}(\boldsymbol{r}) = (\boldsymbol{B} \times \boldsymbol{r})/2 + \tilde{\boldsymbol{A}}(\boldsymbol{r})$, where the magnetic induction $\boldsymbol{B} = (0, 0, B)$

is the field averaged over the vortex lattice cell and $\tilde{\boldsymbol{A}}(\boldsymbol{r})$ represents the variable part of the field which is periodic in the vortex lattice and has zero spatial average. The unit vectors of the triangular vortex lattice are chosen as $\boldsymbol{u}_1 = (a_0, 0, 0)$ and $\boldsymbol{u}_2 = (\frac{1}{2}a_0, \sqrt{3}a_0/2, 0)$, where the intervortex spacing is $a_0 = (2\phi_0/\sqrt{3}B)^{1/2}$. We use periodic boundary conditions for the unit cell of the vortex lattice and take into account the order parameter phase winding around each vortex[21].

Throughout the paper, we employ Eilenberger units for the first band if it would have been single ($V_{12} = V_{22} = 0$): $R_1 = \hbar v_1/2\pi T_{c,1}$ is taken as a unit length ($R_1 \approx 0.88\,\xi_{01}$ where ξ_{01} is the zero-T BCS coherence length of the "bare" first band). Fermi velocities are normalized to v_1, the magnetic field is measured in units of $B_1 = \phi_0/2\pi R_1^2$ and the current density in $cB_1/4\pi R_1$, the energy unit is $\pi T_{c,1}$, and $T_{c,1}$ is the transition temperature in the single-band limit. In these units, Eqs. (2) and (5) take the form:

$$(\omega + \boldsymbol{v}_\alpha \cdot \boldsymbol{\nabla}) f_\alpha = \Delta_\alpha g_\alpha - i\boldsymbol{v}_\alpha \cdot [(\boldsymbol{B} \times \boldsymbol{r})/2 + \tilde{\boldsymbol{A}}] f_\alpha \,, \quad (7)$$

$$\boldsymbol{J}_\alpha(\boldsymbol{r}) = -\frac{2T}{\kappa_1^2} \sum_{\omega>0} \langle \boldsymbol{v}\, \mathrm{Im}\, g(\omega, \boldsymbol{k}, \boldsymbol{r}) \rangle_\alpha \,. \quad (8)$$

Hereafter we keep the same notation for dimensionless quantities as for their dimensional counterparts; we will indicate explicitly if common units are needed.

The quantity $\kappa_1 = \phi_0 T_{c,1}/\pi\hbar^2 v_1^2 \sqrt{2N_0}$ has the same order of magnitude as the GL parameter for one-band isotropic case, $\kappa_{GL} = 3\phi_0 T_c/\hbar^2 v^2 \sqrt{7\zeta(3)N(0)}$. However, κ_1 does not have the meaning of the penetration-depth-to-coherence-length ratio for the two-band system[2,3], rather it is a convenient dimensionless material parameter.

The dimensionless self-consistency equations take the form:

$$\Delta_\alpha(\boldsymbol{r}) = 2tN_0V_{11} \sum_{\beta,\,\omega} \frac{V_{\alpha\beta}}{V_{11}} \langle f(\omega, \boldsymbol{k}, \boldsymbol{r}) \rangle_\beta \,, \quad (9)$$

$$\pi e^{-\gamma} T_{c,1} = 2\omega_D \exp(-1/N_0V_{11}) \,, \quad t = T/T_{c,1} \quad (10)$$

where γ is the Euler constant. In our calculations we set the cutoff frequency $\omega_D = 40\,T_{c,1}$ and $\kappa_1 = 4$. The numerical procedure is outlined in Appendix A.

The profiles of the pairing amplitudes $|\Delta_\alpha(\boldsymbol{r})|$ in real space are fitted by a 5$^{\text{th}}$-order polynomial near the vortex center along the nearest neighbor vortex direction. We estimate the vortex core size $\xi_\alpha^{(c)}$ from

$$\Delta_\alpha(\boldsymbol{r}) = \Delta_{\mathrm{m},\alpha} \frac{r}{\xi_\alpha^{(c)}} + O(r^2) \,, \quad j = 1, 2 \quad (11)$$

near the vortex center. $\Delta_{\mathrm{m},\alpha}$ is the maximum value of $|\Delta_\alpha(\boldsymbol{r})|$ within the unit cell.

III. V_{12} OF THE SAME ORDER AS V_{11}

First, we present our results for $V_{12} = 0.32V_{11}$. In order to see the effect of the coupling in the second band, we consider two cases: $V_{22} = 0$ and $V_{22} = 0.32V_{11}$.

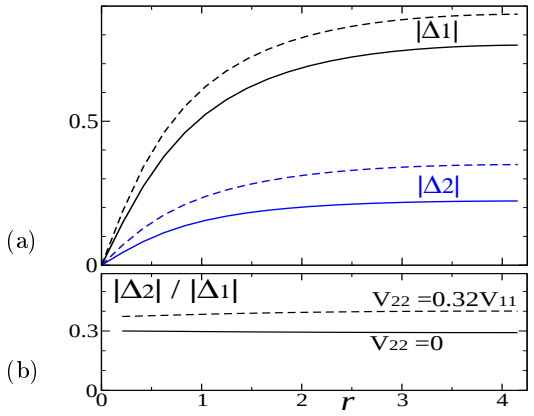

FIG. 1. (Color online) (a) Pairing amplitudes $|\Delta_1(\boldsymbol{r})|$ and $|\Delta_2(\boldsymbol{r})|$ (in units $\pi T_{c,1}$) vs distance r (in units of $R_1 = \hbar v_1/2\pi T_{c,1}$) from the vortex center to the midpoint between nearest neighbor vortices. In this calculation, $V_{12}/V_{11} = 0.32$, $t = T/T_{c,1} = 0.5$, and $B = 0.1$ (in units $\phi_0/2\pi R_1^2$). Solid lines are for $V_{22} = 0$, dashed lines are for $V_{22}/V_{11} = 0.32$. (b) Nearly constant ratios $|\Delta_2(\boldsymbol{r})|/|\Delta_1(\boldsymbol{r})|$ imply the same length scales for both pairing amplitudes.

The profiles of $|\Delta_1(\boldsymbol{r})|$ and $|\Delta_2(\boldsymbol{r})|$ are shown in Fig. 1(a). Near the vortex center, both $|\Delta_1(\boldsymbol{r})|$ and $|\Delta_2(\boldsymbol{r})|$ recover over the same lengths; this is seen most directly in panel (b) where nearly constant ratios $|\Delta_2(\boldsymbol{r})|/|\Delta_1(\boldsymbol{r})|$ are shown. In the presence of finite intraband coupling of the second band V_{22}, the amplitude of the pair potential of this band increases, with $|\Delta_2(\boldsymbol{r})|/|\Delta_1(\boldsymbol{r})| \sim 0.4$, as expected. The spatial dependence of the two pair potentials is however the same.

Temperature dependences of the core radii $\xi_\alpha^{(c)}$ and of the maximum value $\Delta_{\mathrm{m},\alpha}$ are given in Fig. 2. While $\Delta_{\mathrm{m},\alpha}$ are slightly smaller than those in zero field (dotted line) as they should, the T-dependence of $\Delta_{\mathrm{m},\alpha}$ is similar to that at zero field. Nearly constant ratios $\Delta_{\mathrm{m},2}/\Delta_{\mathrm{m},1}$ are ≈ 0.3 for $V_{22} = 0$ and ≈ 0.4 for $V_{22} = 0.34V_{11}$. As the temperature increases, this ratio changes little: from 0.291 to 0.295 for $V_{22} = 0$, and from 0.406 to 0.392 for $V_{22} = 0.32V_{11}$, respectively. Within our analysis we also reproduce Kramer-Pesch shrinking of the vortex core sizes $\xi^{(c)}$ on cooling[22–24], see Fig. 2(c,d). Thus, we obtain $\xi_2^{(c)} \approx \xi_1^{(c)}$ in the whole temperature range. While it is expected that $\xi_2^{(c)}/\xi_1^{(c)} \to 1$ for $T \to T_c$, our finding of numerically very similar length scales over a broad temperature regime is rather surprising.

The field dependencies of the pairing amplitudes and deduced length scales are shown in Fig. 3. As expected, the $\Delta_{\mathrm{m},\alpha}$ are suppressed upon increasing the magnetic field, see Fig. 3(a). As shown in Fig. 3(b,c), after a slow decrease at low B's, the core radii $\xi_\alpha^{(c)}$ are once again nearly constant over a wide range of field values. Most importantly however, we find at all fields that $\xi_1^{(c)} \approx \xi_2^{(c)}$,

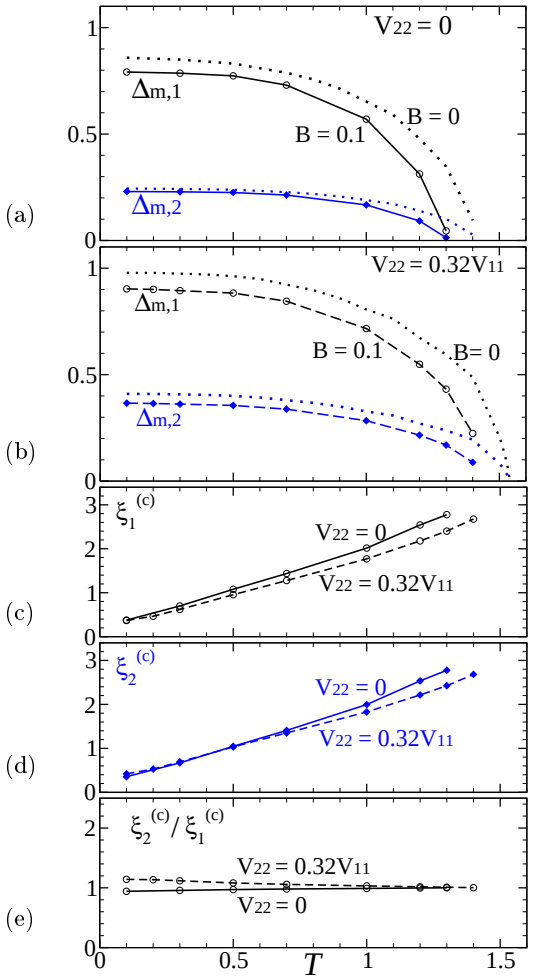

FIG. 2. (Color online) (a) Temperature dependence of maximum values $\Delta_{\mathrm{m},\alpha}$ of pairing amplitudes $|\Delta_\alpha(\boldsymbol{r})|$ at $B = 0.1$ for $V_{22} = 0$ and $V_{12} = 0.32\,V_{11}$. Zero-field $|\Delta_\alpha|$ are shown by dotted lines. (b) The same as (a) for $V_{22} = 0.32V_{11}$. (c,d) T dependences of core sizes $\xi_\alpha^{(c)}$, and (e) of $\xi_2^{(c)}/\xi_1^{(c)}$ for $B = 0.1$. Temperature T is in units of $T_{c,1}$.

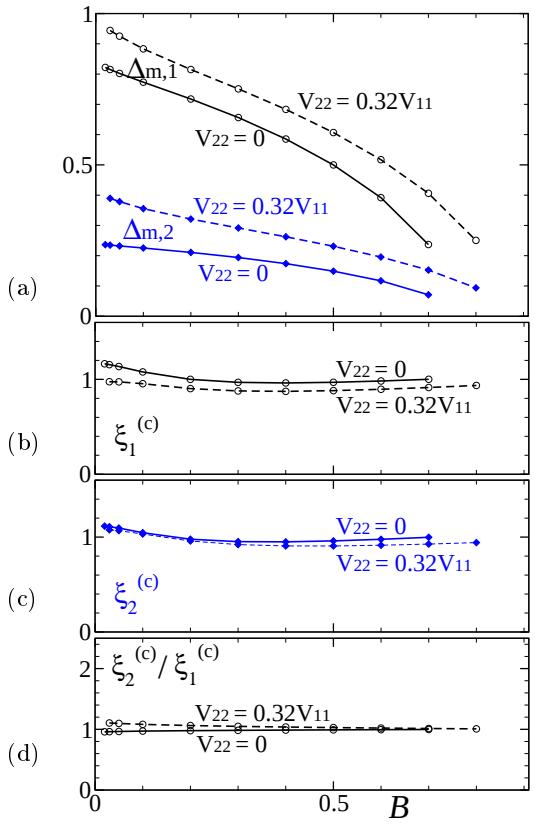

FIG. 3. (Color online) (a) Magnetic field dependence of $\Delta_{\mathrm{m},\alpha}$, $\alpha = 1, 2$. (b,c) B dependence of the core sizes $\xi_\alpha^{(c)}$ and (d) the ratio $\xi_2^{(c)}/\xi_1^{(c)}$. Inputs: $t = 0.5$, $V_{12} = 0.32V_{11}$, solid lines are for $V_{22} = 0$, dashed lines for $V_{22} = 0.32V_{11}$.

see panel (d) of Fig. 3. As B approaches the upper critical field H_{c2}, $\xi_2^{(c)}/\xi_1^{(c)} \to 1$, see Fig. 3(d). This conclusion agrees with the two-band theory of H_{c2}[25], where it has been shown that near the second order phase transition at H_{c2}, the two pairing amplitudes satisfy the system of equations $-\xi^2\boldsymbol{\Pi}^2\Delta_\alpha = \Delta_\alpha$ with the same ξ.

IV. DECOUPLING LIMIT $V_{12} \ll V_{11}$

Next we analyze the regime of almost decoupled band. In this limit, the two superconducting condensates are nearly independent. The vortex core radii can be different and dependent on the characteristics of the bands[6,7].

We assume that the second band has pairing interaction $V_{22} = 0.85V_{11}$. This gives superconducting tran-

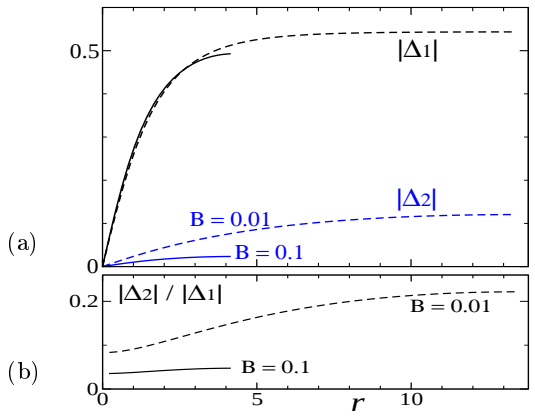

FIG. 4. (Color online) (a) $|\Delta_1(\boldsymbol{r})|$ and $|\Delta_2(\boldsymbol{r})|$ vs distance r from the vortex center to the midpoint between nearest neighbor vortices. (b) $|\Delta_2(\boldsymbol{r})|/|\Delta_1(\boldsymbol{r})|$. Input parameters are $V_{12} = 0.01V_{11}$, $V_{22} = 0.85V_{11}$, and $t = 0.5$; solid lines are for $B = 0.1$, dashed lines are for $B = 0.01$.

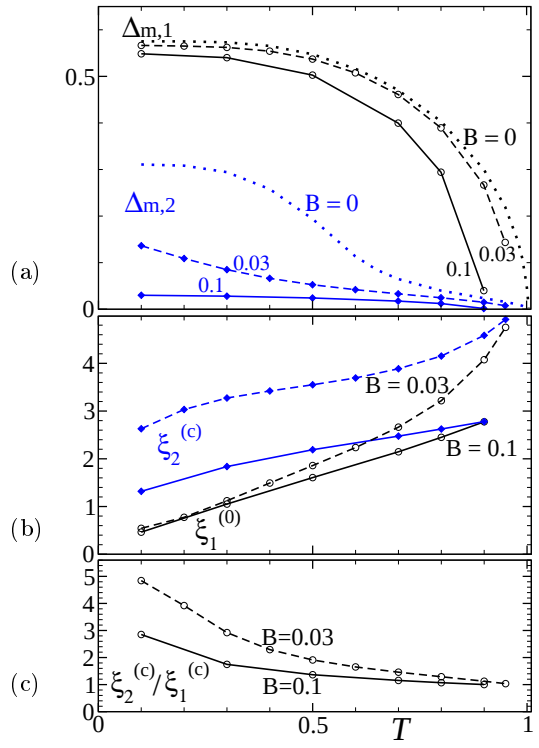

FIG. 5. (Color online) (a) Temperature dependence of $\Delta_{\mathrm{m},\alpha}$ at $B = 0$ (dotted lines), $B = 0.03$ (dashed lines), and $B = 0.1$ (solid lines). (b) T dependence of the vortex core radii $\xi_1^{(c)}$ and $\xi_2^{(c)}$, and (c) the ratio $\xi_2^{(c)}/\xi_1^{(c)}$. $V_{12} = 0.01V_{11}$ and $V_{22} = 0.85V_{11}$.

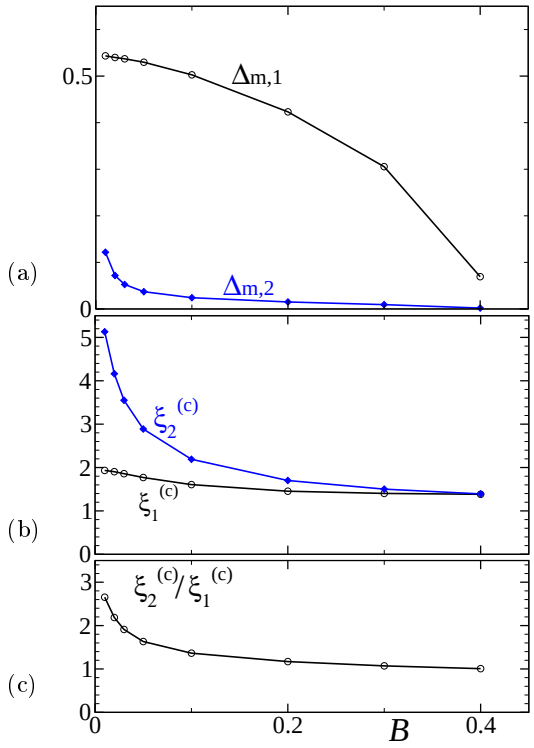

FIG. 6. (Color online) (a) The field dependence of $\Delta_{\mathrm{m},\alpha}$. (b) B-dependence of core radii $\xi_1^{(c)}$ and $\xi_2^{(c)}$, and (c) the ratio $\xi_2^{(c)}/\xi_1^{(c)}$. Input parameters: $t = 0.5$, $V_{12} = 0.01V_{11}$ and $V_{22} = 0.85V_{11}$.

sition temperature $T_{c,2} \sim 0.51T_{c,1}$ and the upper critical field $H_{c2,2} \sim 0.025$ at $T = 0.1T_{c,1}$ in the second band, when the interband coupling is absent, $V_{12} = 0$. Hereafter, we study the vortex core size when a weak interband coupling exists as $V_{12} = 0.01V_{11}$. The resulting $|\Delta_\alpha(\boldsymbol{r})|$ are presented in Fig. 4(a). At a low field $B = 0.01$ (dashed lines), the recovery of $|\Delta_2(\boldsymbol{r})|$ with increasing r is indeed slow compared to $|\Delta_1(\boldsymbol{r})|$, and as a result we find that $\xi_2^{(c)} > \xi_1^{(c)}$. This behavior can also be seen in the r dependence of the ratio $|\Delta_2(\boldsymbol{r})|/|\Delta_1(\boldsymbol{r})|$, which is no longer constant, but decreases near the vortex core, see Fig. 4(b). For higher field, $B = 0.1$ (see the solid lines in Fig. 4), $|\Delta_1(\boldsymbol{r})|$ within the core region does not change substantially compared to the low-field case, whereas $|\Delta_2(\boldsymbol{r})|$ is suppressed strongly, as the intervortex distance is too short for the recovery of $|\Delta_2(\boldsymbol{r})|$. In other words, since the "effective H_{c2}" of the bare second band is small due to a larger coherence length ($v_2 = 3v_1$ and Δ_2 is small), superconductivity of the second band is easily suppressed by magnetic fields. Hence, at high fields, the contribution to superconductivity of the second band is weak.

The corresponding temperature dependence of the nearly decoupled band regime is shown in Fig. 5. $\Delta_{\mathrm{m},1}$ has the typical T-dependence of the BCS theory. However, $\Delta_{\mathrm{m},2}(T)$ is different. At low T, the superconductivity of the second band is enhanced, since it is caused here by $V_{22} = 0.85\,V_{11}$. For $B = 0$, Δ_2 is very small at elevated temperatures. Above the intrinsic transition temperature of the decoupled second band, superconductivity of this band is only induced by the weak interband coupling V_{12}, an observation that was made already shortly after the formulation of the BCS-theory[26]. With increasing B, the enhancement of $\Delta_{\mathrm{m},2}$ at low T disappears and practically vanishes at $B = 0.1$. The B-dependence of the pairing amplitudes are shown in Fig. 6. $\Delta_{\mathrm{m},2}$ decreases rapidly at low B reflecting small effective $H_{c2,2}$ of the second band, and remains small at higher B due to weak coupling V_{12}. In the high B range, $\xi_1^{(c)} \approx \xi_2^{(c)}$. This combination of field and temperature variation of nearly decoupled bands may serve as a tool to identify whether one is indeed in this limit.

We note that the Kramer-Pesch shrinking of $\xi_2^{(c)}$ on cooling is weak compared to that of $\xi_1^{(c)}$, see Fig. 5(b). Thus, the ratio $\xi_2^{(c)}/\xi_1^{(c)}$ increases upon lowering T. On the other hand, at higher T and for fields approaching H_{c2}, $\xi_2^{(c)}/\xi_1^{(c)} \to 1$ (again in agreement with Ref.[25]).

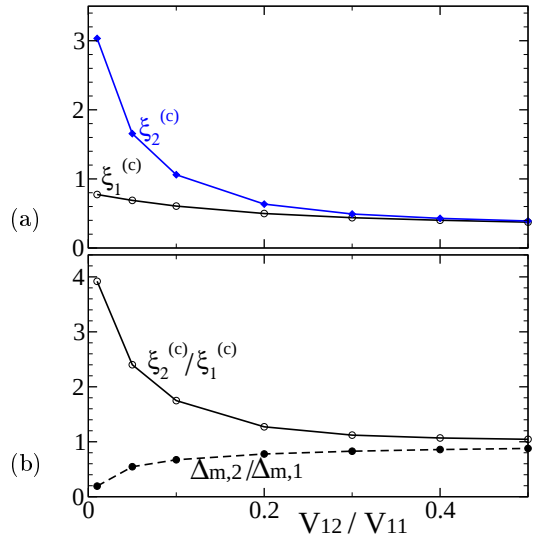

FIG. 7. (Color online) (a) $\xi_\alpha^{(c)}$ vs interband coupling V_{12}/V_{11} for $V_{22} = 0.83\,V_{11}$ at $t = 0.2$ and $B = 0.03$. (b) Ratios $\xi_2^{(c)}/\xi_1^{(c)}$ and $\Delta_{m,2}/\Delta_{m,1}$ vs V_{12}/V_{11} for the same parameters as (a).

V. DISCUSSION

The issue of the spatial variation of the superconducting order parameter in multiband systems is interesting and relevant, in particular because of an increasing number of physical systems that clearly display multiband behavior in their superconducting properties. In addition to the description of the variation of the order parameter near vortex cores, the DOS distribution is related to $\Delta(\boldsymbol{r})$ and is measurable. Recent STM low-T data, interpreted within a phenomenological model, suggest that $\xi_1^{(c)} \approx \xi_2^{(c)}$[17]. While such a behavior (we call it "length-scales locking") is to be expected in the immediate vicinity of the transition temperature, it is not obvious away from T_c. Thus, a microscopic analysis of this question is timely and relevant. It shows that, within the accuracy of our numerical routine, $\xi_1^{(c)} \approx \xi_2^{(c)}$ if the interband coupling is of the same order as intraband ones. This conclusion turns out to be valid at all temperatures and fields. In agreement with other microscopic calculations[6,7], we find this rule is violated for a very weak interband coupling when the system is close to the limit of nearly decoupled condensates. The peculiar field and temperature dependence of such nearly decoupled bands can easily be used to test, for a given material, whether the coupling between bands is weak or only moderate.

To make this statement more quantitative, we show in Fig. 7 the ratio $\xi_2^{(c)}/\xi_1^{(c)}$ as a function of the interband coupling V_{12}/V_{11} at fixed $t = T/T_{c,1} = 0.2$ and $B = 0.03$. One sees that this ratio exceeds the value of 2 only when roughly $V_{12}/V_{11} < 0.1$. As discussed above, MgB_2 can be very well described by $V_{12}/V_{11} \approx 0.2$ (see Refs.[9,11–14]). Thus, we conclude that this systems is not in the regime where two distinct characteristic length scales emerge.

In conclusion, by solving the quasi-classical Eilenberger equations, we analyzed the spatial variation of the pairing amplitudes within the vortex lattice of a two band superconductor over a wide range of temperatures and magnetic fields. Near the superconducting transition temperature $T_c(B)$ at a field B, it is established[1–3,25] that the emergence of one order parameter in a two-band system naturally implies that the spatial variation of this order parameter is governed by a single length scale. Away from T_c (and generally from the curve $H_{c2}(T)$) it is however expected that for a sufficiently weak coupling between the bands, distinct characteristic length scales for the respective pairing amplitudes emerge. Here we showed that such decoupling of the length scales occurs for values of the interband pairing interaction V_{12} that are less than one order of magnitude of the largest intraband coupling. For larger values of the interband coupling a common temperature and field variation of the length $\xi_1^{(c)}$ and $\xi_2^{(c)}$ of the pairing amplitudes sets in. What is most surprising about these results is that these two length scales not only follow a common T-dependence, they are practically identical in their magnitude, $\xi_1^{(c)} \approx \xi_2^{(c)}$. In other words, we observe a robust length scale locking of moderately coupled multiband superconductors. Whatever difference might there be in the values of the length scales of the uncoupled system, our analysis shows that this difference is most likely to disappear everywhere below $H_{c2}(T)$ (see also Appendix B).

In this work we considered only clean two-band systems. Usually, the impurity scattering is expected to cause isotropization of superconducting characteristics. Hence, we do not expect scattering to amplify differences of the length scales $\xi_\alpha^{(c)}$. Still, as discussed in Ref. [16], interband scattering can cause the superconductivity to become gapless with two bands acquiring substantially different DOSs in superconducting state. The question of how this difference affects $\xi_\alpha^{(c)}$ remains to be addressed. Also, our work does not cover all possible differences in band parameters which may lead to measurable differences in $\xi_1^{(c)}$ and $\xi_2^{(c)}$. For example, if one of the bands is shallow and nearly empty[29], the ratio of Fermi velocities might be large enough to overcome the locking effect.

ACKNOWLEDGEMENTS

We thank L. Boulaevskii, A. Vagov, A. Shanenko, M. Milošević, H. Suderow, and E. Babaev for illuminating comments. Work of V.K. was supported by the U.S. Department of Energy, Office of Science, Basic Energy Sciences, Materials Sciences and Engineering Division. The Ames Laboratory is operated for the U.S. DOE by Iowa State University under Contract No. DE-AC02-07CH11358.

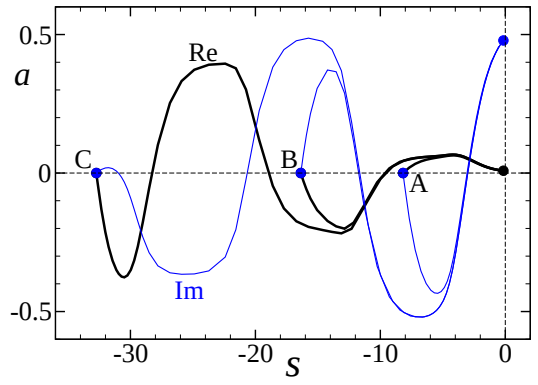

FIG. 8. (Color online) Solving the first-order ordinary differential Eq. (A2) along the trajectory $\boldsymbol{r}' = \boldsymbol{r} + s\hat{\boldsymbol{v}}_\alpha$ for a at $s = 0$. Real and imaginary part of a are shown for start positions $s_0 = -8.2$ (A), -16.4 (B) and -32.7 (C). It is seen, that a converges to the same solution at $s = 0$. Input parameters are $\phi = 1.25°$ for $\boldsymbol{k}$, $\alpha = 1$, $\omega = \pi T$ and $V_{22} = 0$ in the case of Fig. 1. $\boldsymbol{r}$ is near the midpoint $(-a_0/2, 0)$ between nearest neighbor vortices.

Appendix A: Numerical method

We briefly summarize the numerical approach to solve the coupled Eilenberger equations Eqs. (2). For the numerical analysis, it is more convenient to employ instead of the function f and g the functions a and b defined via

$$f = \frac{2a}{1+ab}, \quad f^+ = \frac{2b}{1+ab}, \quad g = \frac{1-ab}{1+ab} \tag{A1}$$

and transform the system (2)-(3) to Ricatti differential equations,

$$\boldsymbol{v}\cdot\boldsymbol{\nabla}a = \left(\Delta - \Delta^* a^2\right) - (\omega + i\boldsymbol{v}\cdot\boldsymbol{A})a, \tag{A2}$$

$$-\boldsymbol{v}\cdot\boldsymbol{\nabla}b = \left(\Delta^* - \Delta b^2\right) - (\omega + i\boldsymbol{v}\cdot\boldsymbol{A})b, \tag{A3}$$

for each band α[27]. Unlike the original Eqs. (2), the equations for a and b are decoupled. The Ricatti equations are then solved by numerical integration along trajectories parallel to the vector $\boldsymbol{v}$[28]. Choosing length $|s_0|$ of these trajectories in Fig. 8, we confirm that the solution does not change when this length is increased. We iterate the set of equations until self-consistent results are obtained.

Appendix B: Simple example of lengths locking

Consider the simplest possible coupling with all components of $V_{\alpha\beta}$ equal to V_0:

$$V_{\alpha\beta} = V_0\left(\delta_{\alpha\beta} + \sigma_{\alpha\beta}\right), \quad \sigma_{\alpha\beta} = \left\{\begin{array}{cc} 0 & 1 \\ 1 & 0 \end{array}\right\}. \tag{B1}$$

Then, the self-consistency relations,

$$\begin{aligned}\Delta_\alpha(\boldsymbol{r}) &= 4\pi T N_0 \sum_{\beta,\,\omega>0}^{\omega_D} V_{\alpha\beta}\langle f(\omega,\boldsymbol{r})\rangle_\beta \\ &= 4\pi T N_0 V_0 \sum_{\beta,\,\omega>0}^{\omega_D} \left(\langle f\rangle_\alpha + \sigma_{\alpha\beta}\langle f\rangle_\beta\right), \end{aligned} \tag{B2}$$

translate to

$$\begin{aligned}\Delta_1(\boldsymbol{r}) &= 4\pi T N_0 V_0 \sum_{\omega>0}^{\omega_D} \left(\langle f\rangle_1 + \langle f\rangle_2\right), \\ \Delta_2(\boldsymbol{r}) &= 4\pi T N_0 V_0 \sum_{\omega>0}^{\omega_D} \left(\langle f\rangle_2 + \langle f\rangle_1\right). \end{aligned} \tag{B3}$$

Thus, $\Delta_1(\boldsymbol{r}) = \Delta_2(\boldsymbol{r})$ exactly for any Fermi velocities, any T and H. In particular, this means $\xi_1^{(c)} = \xi_2^{(c)}$.

It is worth noting that this conclusion follows from the self-consistency equations without actually solving Eilenberger equations for f_α. It is readily shown that for the coupling matrix of the form (B1) the same result can be obtained for unequal normal band DOS'.

* ichioka@okayama-u.ac.jp

[1] B. T. Geilikman, R. O. Zaitsev, and V. Z. Kresin, Sov. Phys. Solid State **9**, 642 (1967).
[2] J. Geyer, R. M. Fernandes, V. G. Kogan, and J. Schmalian, Phys. Rev. B **82**, 104521 (2010).
[3] V. G. Kogan and J. Schmalian, Phys. Rev. B **83**, 054515 (2011).
[4] E. Babaev and M. Speight, Phys. Rev. B **72**, 180502 (2005).
[5] E. Babaev, J. Calström, M. Silaev, and J.M. Speight, arXiv:1608.02211.
[6] L. Komendova, Yajiang Chen, A. A. Shanenko, M.V. Milošević, and F. M. Peeters, Phys. Rev. Lett. **108**, 207002 (2012).
[7] M. Silaev and E. Babaev, Phys. Rev. B **84**, 094515 (2011).
[8] A. Vagov, A. A. Shanenko, M. V. Milošević, V. M. Axt, and F. M. Peeters Phys. Rev. B**86**, 144514 (2012).
[9] I. I. Mazin and V. P. Antropov, Physica C **385**, 49 (2003).
[10] G. Blumberg, A. Mialitsin, B. S. Dennis, M. V. Klein, N. D. Zhigadlo, and J. Karpinski, Phys. Rev. Lett. **99**, 227002 (2007).
[11] A.Y. Liu, I. I. Mazin and J. Kortus, Phys. Rev. Lett., **87**, 087005 (2001).
[12] A. A. Golubov, J. Kortus, O. V. Dolgov, O. Jepsen, Y. Kong, O. K. Andersen, B. J. Gibson, K. Ahn and R. K. Kremer, J. Phys.: Condens. Matter **14**, 1353 (2002).
[13] H. J. Choi, D. Roundy, H. Sun, M. L. Cohen, and S. G. Louie, Phys. Rev. B **66**, 020513 (2002).
[14] H. J. Choi, D. Roundy, H. Sun, M. L. Cohen, and S. G. Louie, Nature **418**, 758 (2002).

[15] I. I. Mazin and J. Schmalian, Phys. C: Supercond. **469**, 614 (1995).
[16] V. G. Kogan and R. Prozorov, Phys. Rev. B **93**, 224515 (2016).
[17] A. Fente, E. Herrera, I. Guillamon, H. Suderow, S. Mañas-Valero, M. Galbiati, E. Coronado and V. G. Kogan, Phys. Rev. B **94**, 014517 (2016).
[18] A. Fente, W. R. Meier, T. Kong, V.G. Kogan, S. L. Bud'ko, P. C. Canfield, I. Guillamon, H. Suderow, arXiv:1608.00605.
[19] M. Ichioka, K. Machida, N. Nakai, and P. Miranović, Phys. Rev. B **70**, 144508 (2004).
[20] G. Eilenberger, Z. Phys. **214**, 195 (1968).
[21] M. Ichioka, N. Hayashi, and K. Machida, Phys. Rev. B **55**, 6565 (1997).
[22] L. Kramer and W. Pesch, Z. Phys. **269**, 59 (1974).
[23] M. Ichioka, N. Hayashi, N. Enomoto, and K. Machida Phys. Rev. B **53**, 15316 (1996).
[24] A. Gumann, S. Graser, T. Dahm, and N. Schopohl, Phys. Rev. B **73**, 104506 (2006).
[25] V. G. Kogan and R. Prozorov, Rep. Prog. Phys. **75**, 114502 (2012).
[26] H. Suhl, B. T. Matthias, and L. R. Walker, Phys. Rev. Lett. **3**, 552 (1959).
[27] N. Schopohl and K. Maki, Phys. Rev. B **52**, 490 (1995).
[28] P. Miranović, M. Ichioka, and K. Machida, Phys. Rev. B **70**, 104510 (2004).
[29] K. Okazaki, Y. Ito, Y. Ota, Y. Kotani, T. Shimojima, T. Kiss, S. Watanabe, C.-T. Chen, S. Niitaka, T. Hanaguri, H. Takagi, A. Chainani, and S. Shin, Sci. Rep. **4**, 4109 (2014)